

An Integer- N Frequency Synthesizer for Flexible On-Chip Clock Generation

S. Mandal,¹ P. Maj,¹ G. W. Deptuch¹

¹Brookhaven National Laboratory, Upton, NY 11973, USA

E-mail: smandal@bnl.gov

ABSTRACT: A low-power integer- N frequency synthesizer for flexible on-chip clock generation has been designed in 65 nm CMOS technology. The circuit can be programmed to generate two independent low-jitter clocks between 30 MHz and 3 GHz that are locked to a 10-50 MHz reference input. The design uses a phase-locked loop (PLL) with a dual-tuned LC voltage-controlled oscillator (VCO), programmable feedback divider, and dual output dividers. The total power consumption from 1.2 V and 0.8 V supplies is 4.0 mW. Experimental results confirm the functionality of the proposed synthesizer over a wide range of output frequencies.

KEYWORDS: Analogue electronic circuits, Digital electronic circuits, VLSI circuits

ARXIV EPRINT: [1234.56789](https://arxiv.org/abs/1234.56789)

¹Corresponding author.

Contents

1	Introduction	1
2	Circuit Design	1
3	Experimental Results	4
4	Conclusion	5

1 Introduction

High-energy physics experiments designed to detect rare events often require high-data-rate links between readout ASICs and back-end processors over lossy channels, such as radio-pure cables [1–3]. For example, the nEXO experiment [2] will require ~ 400 radio-pure data links, each operating at speeds of 500 Mb/s in a liquid xenon cryostat (165K). The cryogenic environment also imposes a strict power constraint of ~ 15 mW per link [4]. Proposed link designs for such challenging scenarios use the *forwarded clock architecture* shown in Fig. 1(b). In this approach, the data acquisition (DAQ) system transfers a low-frequency reference clock (e.g., from a crystal oscillator) to the analog front-end (AFE) and readout system over a low-speed cable, which is then used by an on-chip frequency synthesizer to generate the high-frequency data-rate clock [5]. Here we describe a low-power integer- N frequency synthesizer suitable for such clock generation applications.

2 Circuit Design

Fig. 1(b) shows a top-level block diagram of the proposed synthesizer. The design uses a phase-locked loop (PLL) with programmable feedback divider and dual output dividers to allow generation of two independent output frequencies. The PLL has a classical structure with an edge-triggered phase-frequency detector (PFD), differential charge pump (CP), passive RC loop filter, voltage-controlled oscillator (VCO), frequency divider, and lock detector (LD). All required biases are generated on-chip via 5-bit current DACs, resulting in a completely self-contained design.

The PFD, which is shown in Fig. 1(c), is based on the design in [6]. It is an efficient implementation of the commonly-used sequential PFD circuit using only NAND gates and inverters. The design is 1) insensitive to input duty cycle; 2) guarantees a minimum up/down (UP/DN) output pulse width in the locked state, thus eliminating any dead zone around the origin of the PFD transfer curve; and 3) has a relatively small delay (three NAND gates) in the critical path.

The CP is shown in Fig. 2. The design uses differential switching to minimize charge injection. An OTA maintains the dummy output voltage (v_{DUMMY}) near the actual output voltage (v_{OUT}) to minimize switching transients. Additionally, a replica-bias loop is used to improve matching between the P- and N-sides, thus reducing phase offset in the locked state. For this purpose, both

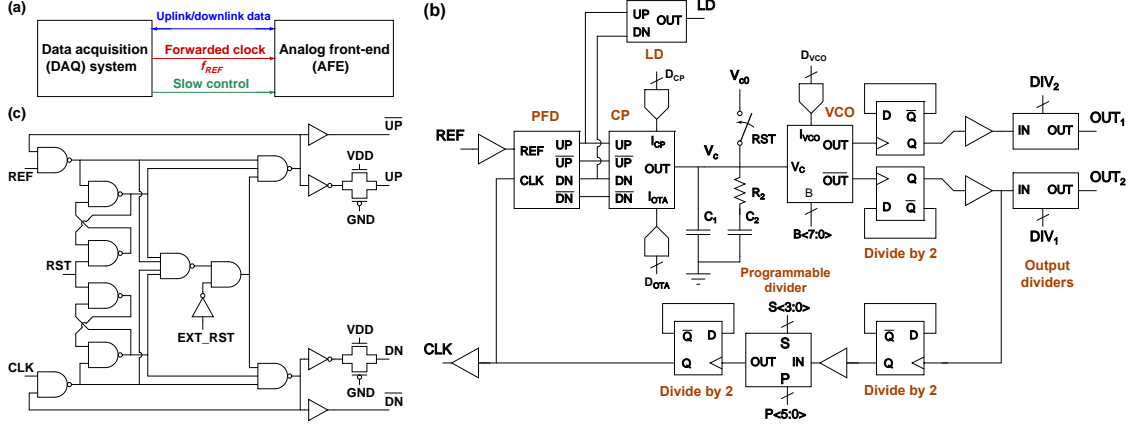


Figure 1. (a) Overview of the forwarded clock architecture. (b) Top-level block diagram of the proposed frequency synthesizer. (c) Schematic of the PFD including reset signals (RST and EXT_RST).

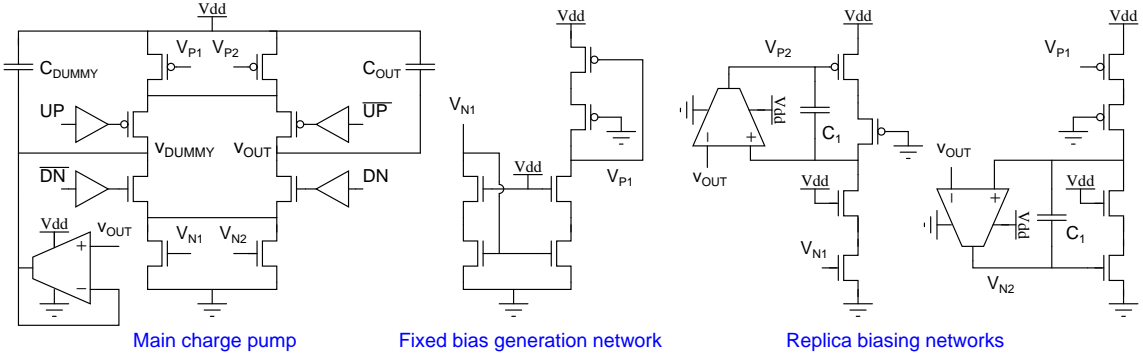


Figure 2. Schematic of the CP, including both the fixed and adaptive biasing networks.

the N- and P-side bias transistors are split into two equal parts. The gate voltages for one part (V_{N1} and V_{P1}) are set by a fixed input current, while those for the other part (V_{N2} and V_{P2}) are adaptively set by a replica biasing network as shown in the figure.

The VCO, which is shown in Fig. 3(a), uses an on-chip LC resonator to minimize phase noise and power supply sensitivity, albeit at the cost of larger die area. The inductor is a center-tapped circular spiral structure, while positive feedback is provided by a cross-coupled NMOS pair. Two levels of frequency tuning are available: coarse tuning (band switching) using 8 equal-valued switched capacitors, and fine tuning using accumulation-mode MOS varactors. The coarse tuning network uses differential switching, as shown in the figure, to minimize the impact of switch on-resistance on tank Q . The switching network includes 1) small NMOS switches to define the V_{DS} of the main switch when it is “on”, and 2) small PMOS switches and series resistors to prevent V_{DS} from exceeding V_{DD} when it is “off”. Phase noise is further minimized by using 1) an RC low-pass filter to remove bias current noise, and 2) an LC tail current filter (tuned to the second harmonic) to reduce $1/f$ noise up-conversion [7]. Power consumption is minimized by operating the VCO at a reduced supply voltage, V_{DDL} . The simulated tuning range for $V_{DDL} = 0.8$ V is 5.6-8.6 GHz with a control gain of ~ 0.6 GHz/V and a typical phase noise of -110 dBc/Hz at 1 MHz offset.

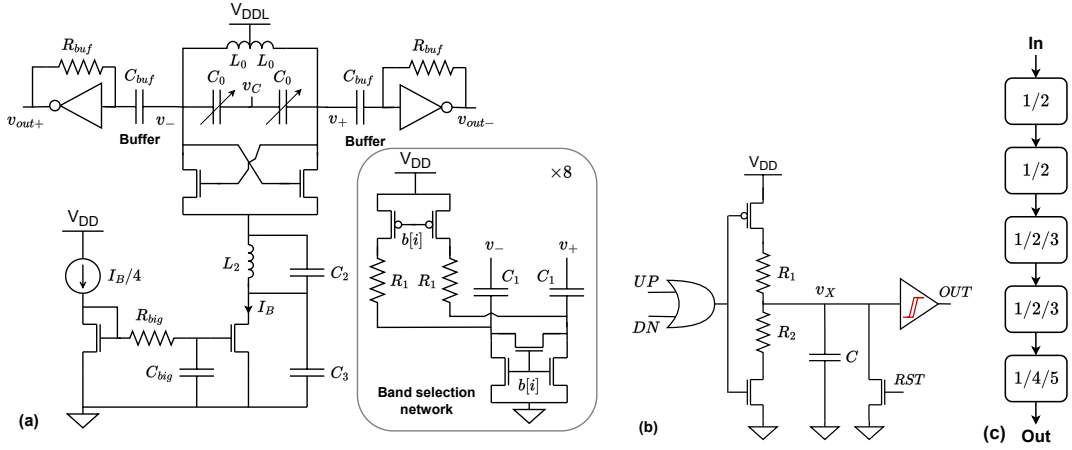


Figure 3. (a) Schematic of the VCO, including both coarse- and fine-tuning networks. (b) Schematic of the lock detector (LD). (c) Block diagram of the output divider.

The VCO outputs are buffered to logic-level signals by AC-coupled CMOS inverters with resistive feedback, as shown in the figure. While this design ensures high gain and insensitivity to the VCO’s output common-mode voltage, it also degrades supply sensitivity since the supply-dependent input capacitance of the inverters contributes to the total capacitance of the LC resonator. This effect can be minimized by running the buffers off a separate low-noise power supply.

The feedback divider uses a pulse-swallow counter topology with a total division ratio of $(NP + S)$, where $N = 2$ is fixed while P and S are adjustable over the ranges 1-63 and 0-15, respectively. Propagation delays are minimized by using dynamic (TSPC) flip-flops within the $N/(N+1)$ dual-modulus prescaler and a one-level carry select adder (CSA) within the programmable counter. The divider output is further divided by 2 to ensure that the recovered clock signal, CLK , has a 50% duty cycle. The second-order passive RC loop filter was optimized for a reference frequency of $f_{REF} = 50$ MHz, a charge pump current of $10 \mu A$, and a loop bandwidth of 230 kHz.

Fig. 3(b) shows a schematic of the lock detector (LD) circuit, which detects when total time-averaged duty cycle of the PFD’s UP and DN outputs, D , is less than a threshold value, D_{min} . In steady-state, charge balance at the node v_x requires $v_x = V_{DD} \left(\frac{D}{1-D} \frac{R_1}{R_2} + 1 \right)^{-1}$. The output of the Schmitt trigger goes high when $v_x \geq \alpha V_{DD}$, its positive-going threshold voltage. Thus, the circuit indicates “lock achieved” when $D \leq D_{min}$, where $D_{min} = \left(\frac{\alpha}{1-\alpha} \frac{R_1}{R_2} + 1 \right)^{-1}$. Note that D_{min} is set by two dimensionless quantities, namely α and R_1/R_2 , and is thus robust to changes in process, voltage, and temperature (PVT). For this design, $\alpha \approx 2/3$ and $R_1/R_2 = 8$, resulting in $D_{min} \approx 0.059$.

Fig. 3(c) shows a block diagram of the programmable output divider. It uses a cascade of selectable divider stages with smaller division ratios, as shown. Each stage also includes a “divide by 1” mode, which is implemented by using a transmission gate multiplexer to bypass the divider circuit. Overall, the design allows a wide range of divide values from 1-160 (including most composite numbers < 32) to be generated while maintaining an output duty cycle close to 50%.

The complete synthesizer uses dual output dividers to allow generation of two programmable output frequencies from the quadrature outputs of the PLL and a standard two-wire I²C serial interface for programming. The overall die area is $450 \mu m \times 500 \mu m$, of which approximately

50% and 25% are occupied by the VCO and main loop filter capacitor, respectively. The nominal power consumption (for $V_{DD} = 1.2$ V and $V_{DDL} = 0.8$ V) is 4.0 mW. As an example, transient noise simulations for $f_{REF} = 40$ MHz and $f_{OUT} = 1.92$ GHz show a bimodal time interval error (TIE) distribution with deterministic and random jitter components [8] of 3.13 ps and 560 fs_{rms}, respectively; the former arises from mismatched rise and fall times of the CMOS output buffers.

3 Experimental Results

Fig. 4(a) shows a die photograph of the fabricated synthesizer ASIC. Due to a shortage of bond pads, all inputs and outputs were encoded as single-ended CMOS signals. Fig. 4(b) summarizes the experimental setup used for room-temperature testing. The test board integrates the ASIC with 1) LVDS drivers and baluns to generate impedance-matched outputs; 2) level translators for the I²C interface; and 3) low-dropout linear voltage regulators (LDOs) for the main and VCO power supplies. The reference input is generated by a GPS-disciplined oscillator (GPSDO). The chosen device (LBE-1420, Leo Bodnar Electronics) has an internal PLL, thus allowing f_{REF} to be easily varied during testing. The I²C parameters are set by a graphical user interface (GUI) implemented on a single-board controller (sbRIO-9629, National Instruments).

The effects of power supply noise and ripple on VCO stability can be analyzed by treating the power supply nodes (V_{DD} and V_{DDL}) as sources of frequency pulling and estimating the resulting control gains, K_{VDD} and K_{VDDL} . For the proposed design, simulations show $K_{VDD} \approx 48$ MHz/V and $K_{VDDL} \approx 380$ MHz/V, respectively, so we focus on the effects of V_{DDL} . The amplitude of the spur generated by a sinusoidal ripple, $v(t) = V_m \sin(2\pi f_m t)$, within V_{DDL} can be shown to be $S_{spur} = 10 \log_{10} \left(\frac{K_{VDDL} V_m}{2 f_m} \right)^2$. This result allows us to estimate the power supply rejection ratio (PSRR) requirements for the LDO. For example, keeping $S_{spur} < -60$ dBc for a 10 mV input ripple at $f_m = 10$ MHz requires PSRR > 36 dB. Similarly, an analytical formula for the effects of supply noise on phase noise (PN) can be obtained by assuming that only white noise sources are significant [9], which is valid in the $1/f^2$ region of the PN spectrum. In this region, the supply-induced PN component is given by $\mathcal{L}_{sup}(\Delta f) = 10 \log_{10} \left(\overline{v_{n,sup}^2}(\Delta f) \left(\frac{K_{VDDL}}{\Delta f} \right)^2 \right)$, where $\overline{v_{n,sup}^2}$ is the power spectral density (PSD) of supply noise and Δf is the offset frequency. Given the VCO's typical phase noise of $\mathcal{L}(\Delta f) \approx -110$ dBc/Hz at $\Delta f = 1$ MHz, we need $\overline{v_{n,sup}^2} < 7.0$ nV/Hz^{1/2} to keep $\mathcal{L}_{sup}(\Delta f) < \mathcal{L}(\Delta f)$, thus limiting degradation of PN to < 3 dB. Accordingly, the board uses one of the few commercial LDOs with low-enough output noise PSD to meet this requirement (Analog Devices LT3042, $\sqrt{\overline{v_n^2}} \approx 2.0$ nV/Hz^{1/2} above 200 Hz).

During initial tests, we set $f_{REF} = 40$ MHz and output divider values of 2 and 8, resulting in output frequencies of 1.92 GHz and 480 MHz, respectively. Eye diagrams and TIE values were measured using the built-in functions provided by a high-speed oscilloscope (Tektronix MSO72004C, 20 GHz bandwidth). Fig. 4(c) shows the measured TIE of the 1.92 GHz output for nominal bias settings. The distribution is well fit by a mixture of Gaussians, i.e., includes both deterministic and random jitter components. Both error terms are significantly larger ($5\times$ to $10\times$) than the simulations due to a combination of 1) reference noise, and 2) added jitter due to single-ended to differential conversion (SEDC) at the inputs of the LVDS driver. The reference input was separately measured to have a random jitter of only 1.25 ps_{rms}, so the non-fundamental SEDC error is dominant.

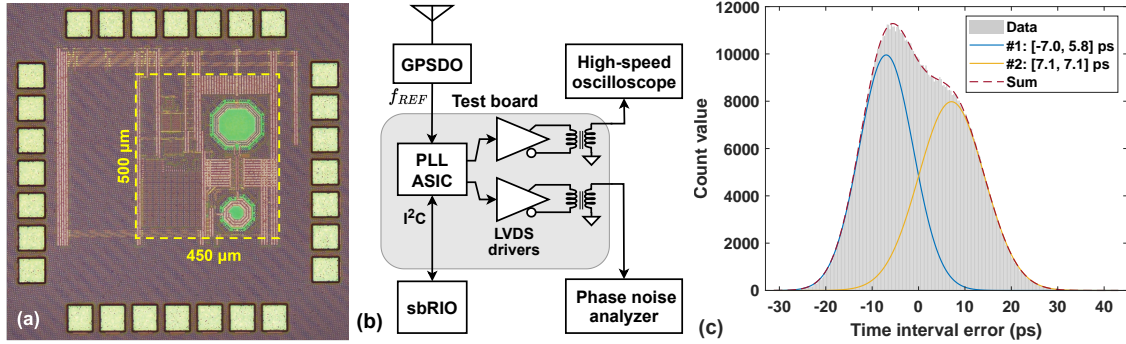


Figure 4. (a) Die photograph of the fabricated test chip. (b) Block diagram of the experimental setup. (c) Measured time interval error (TIE) distribution at an output frequency of 1.92 GHz for $f_{REF} = 40$ MHz.

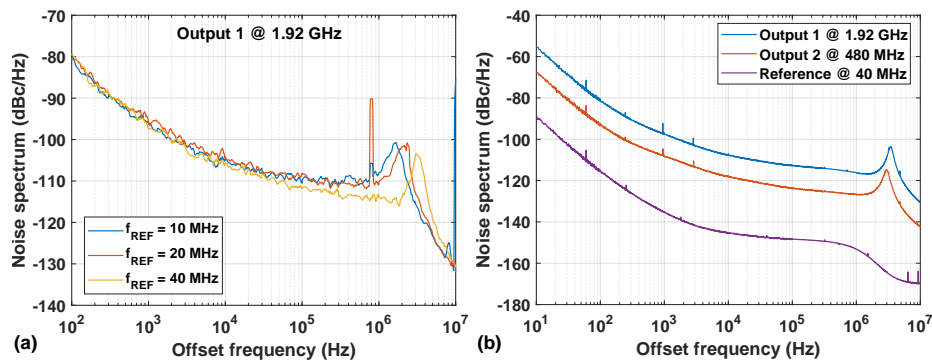


Figure 5. (a) Measured output phase noise (using the spectrum analyzer) at 1.92 GHz for different values of f_{REF} . (b) Measured reference and output phase noise (using the phase noise analyzer) at $f_{REF} = 40$ MHz.

Phase noise measurements were performed using either 1) the phase noise mode of an RF spectrum analyzer (Rohde & Schwarz FSW26), or 2) a dedicated phase noise analyzer (Rohde & Schwarz FSWP50). The latter uses the cross-spectrum method to suppress internal noise sources, resulting in a significantly lower instrument noise floor for a given total measurement time [10]. Fig. 5(a) shows the measured phase noise PSD at 1.92 GHz for three different reference frequencies (10, 20, and 40 MHz). As expected, increases in f_{REF} result in 1) increased loop gain and closed-loop bandwidth; and 2) reduced multiplication of reference phase noise. Fig. 5(b) compares the measured PSDs of the reference and both outputs for a fixed $f_{REF} = 40$ MHz.

4 Conclusion

A low-power integer- N synthesizer suitable for flexible on-chip clock generation has been designed in 65 nm CMOS technology and tested at room temperature (300K). The measured jitter was degraded by the use of single-ended CMOS outputs, but is nevertheless suitable for downlink data transmission up to 3 Gb/s. Future tests will focus on cryogenic operation. For this purpose, the test board will be modified to remove the LDOs since they are unlikely to function at cryogenic temperatures. Instead, they will be included within an auxiliary board kept outside the cryostat.

References

- [1] F. Capozzi, S.W. Li, G. Zhu and J.F. Beacom, *DUNE as the next-generation solar neutrino experiment*, *PRL* **123** (2019) 131803.
- [2] G. Adhikari, S. Al Kharusi, E. Angelico, G. Anton, I. Arnquist, I. Badhrees et al., *nEXO: neutrinoless double beta decay search beyond 10^{28} year half-life sensitivity*, *Journal of Physics G: Nuclear and Particle Physics* **49** (2021) 015104.
- [3] J. Albert, G. Anton, I. Arnquist, I. Badhrees, P. Barbeau, D. Beck et al., *Sensitivity and discovery potential of the proposed nEXO experiment to neutrinoless double- β decay*, *PRC* **97** (2018) 065503.
- [4] N.S. John, S. Mandal, E. Villalpando, P. Maj and G.W. Deptuch, *Testing of a line driver with configurable pre-emphasis on lossy transmission lines*, *IEEE Transactions on Nuclear Science* (2024) .
- [5] S. Biereigel, P. Moreira, S. Kulis, R. Francisco, P.V. Leitaó, P. Leroux et al., *SISSA: The lpGBT PLL and CDR architecture, performance and SEE robustness*, *PoS* (2020) 034.
- [6] I.A. Young, J.K. Greason and K.L. Wong, *A PLL clock generator with 5 to 110 MHz of lock range for microprocessors*, *IEEE Journal of Solid-State Circuits* **27** (1992) 1599.
- [7] E. Hegazi, H. Sjoland and A.A. Abidi, *A filtering technique to lower LC oscillator phase noise*, *IEEE Journal of Solid-State Circuits* **36** (2001) 1921.
- [8] I. Galton and C. Weltin-Wu, *Understanding phase error and jitter: Definitions, implications, simulations, and measurement*, *IEEE Transactions on Circuits and Systems I: Regular Papers* **66** (2018) 1.
- [9] A. Urso, Y. Chen, J.F. Dijkhuis, Y.-H. Liu, M. Babaie and W.A. Serdijn, *Analysis and design of power supply circuits for RF oscillators*, *IEEE Transactions on Circuits and Systems I: Regular Papers* **67** (2020) 4233.
- [10] E. Rubiola and F. Vernotte, *The cross-spectrum experimental method*, *arXiv preprint arXiv:1003.0113* (2010) .